Interaction of nanoparticles with lipid layers

Jonghyun Park and Wei Lu*
Department of Mechanical Engineering, University of Michigan, Ann Arbor, Michigan 48109, USA
(Received 25 April 2009; published 21 August 2009)

Poly (amidoamine) dendrimer nanoparticles are used extensively in diverse biological and medical applications. Examples include gene and drug delivery, where nanoparticles disrupt cell membranes to allow the transport of material into cells. The size and surface chemistry of these particles have a strong effect on their interaction with membranes. This paper proposes a three-dimensional phase-field model to investigate how the interaction drives deformation and morphological evolution of the membrane. Attention is focused on the hole-formation process in the membrane. The simulations have demonstrated that a larger amine-terminated generation 7 dendrimer, which has positive charges, causes the formation of a hole in the membrane. The displaced membrane molecules enclose the particle and form a dendrimer-filled membrane vesicle. The effect is significantly reduced for a smaller dendrimer. An acetamide-terminated dendrimer, which has a neutral charge at the surface, does not cause hole formation. These results agree with experimental observations from atomic force microscopy. The study will provide insight into the design of appropriate nanoparticle surface properties for medical applications.

DOI: 10.1103/PhysRevE.80.021607 PACS number(s): 68.43.Hn, 68.35.Md

I. INTRODUCTION

Dendrimers are a new class of branched, synthetic macromolecules with layered architectures that show promises in diverse biomedical applications such as gene therapy and targeted drug delivery [1,2]. A dendrimer consists of a series of chemical shells, each called a generation, built on a small core molecule. The core molecule is referred to as generation 0 or G0. Each successive repeat unit along all branches forms the next generation. Poly(amidoamine) (PAMAM) dendrimers, in particular, have been considered to be very promising for biomedical applications because of their excellent monodispersity, well-defined mass and size, and surfaces that are chemically functionalized [3,4]. The successful application of PAMAM dendrites requires a fundamental understanding of how they interact with cell membranes and cause deformations. To understand the biocompatibility of dendrimers, experiments have been carried out to investigate their interaction with lipid vesicles and cultured cells. [5,6] An interesting finding is that dendrimers are able to cause disruption of membranes. The interaction becomes stronger for dendrimers of higher generations carrying positive charges. These nanoparticles appear inherently nonselective and that the nanosize scale might play a role in how they nonselectively affect the membrane. Using atomic force microscopy, enzyme assays, and fluorescence microscopy, Hong *et al.* [7,8] observed that amine-terminated generation 7 (G7) PAMAM dendrimers caused the formation of holes in aqueous supported lipid bilayers, whereas acetylated dendrimers (generation 5, G5) did not cause holes but would expand pre-existing holes. These observations suggest that the surface end group plays an important role in the interactions. Orr and co-workers [7,9] investigated DMPC-supported lipid bilayers by atomic force microscopy (AFM). They observed that the dendrimer size also influenced the interaction with lipid bilayers. Higher-generation dendrimers caused formation and growth of holes, whereas the ability to remove lipids from bilayer was reduced for lower-generation dendrimers. In addition, they also found the effect of surface chemistry on the propensity for hole formation, which is similar to the observation of Hong *et al.* [7,8].

Theoretical models and computer simulations are useful tools to elucidate the interaction between dendrimers and membranes. Molecular dynamics simulations [10,11] can reveal atomistic details but are restricted to small length and time scales. To overcome the limitations, Lee and Larson [12] proposed a coarse-grained model and applied it to study generation 3 (G3) and G5 PAMAM dendrimers. The simulation has revealed interaction dynamics up to 0.5 μs. Currently, the calculation for larger systems such as G7 dendrimer and explicit water solvation is still too computationally demanding. Experiments have shown that the typical time scale for the process is minutes, which requires further alleviation of the time scale constraint. Our objective in the present work is to elucidate the interactions between dendrimer and membrane with a continuum model and provide the physical understanding from the fundamentals of thermodynamics. We adopt a phase-field approach, which has recently emerged as a powerful computational method to model morphological and microstructure evolutions in material [13,14] and biological systems [15]. The evolution proceeds to reduce the total free energy of a system, which can incorporate energetics of multiple physical origins. The dendrimer nanoparticles studied in this research include G7 dendrimer and G5 dendrimer. They have two types of end groups: amine-terminated dendrimer which has positive charges on the surface and acetamide-terminated dendrimer which is charge neutral on the surface.

II. MODELING

The nonselective behavior suggests that a uniform mechanism may exist to describe how nanoparticles induce the hole

*Corresponding author. FAX: +1734 647 3170; weilu@umich.edu

 ©2009 The American Physical Society

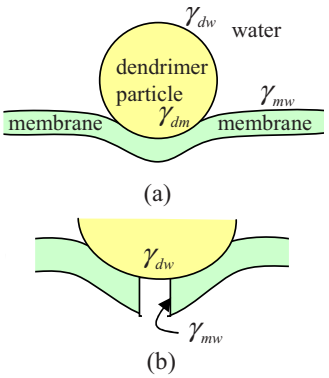

FIG. 1. (Color online) (a) A schematic of the particle/membrane setup. (b) Formation of a hole in the membrane.

formation in membranes. Here, we show that the competitive energetics and mass transport kinetics may explain the behavior. Consider the setup shown in Fig. 1(a). Lump the interatomic and surface charge interactions between the nanoparticle and the membrane into an interfacial tension term γ_{dm}. When γ_{dm} is lower than $\gamma_{dw}+\gamma_{mw}$, i.e., the interfacial tension of particle/water and membrane/water, it is energetically favorable for the membrane to wrap the particle. However, the wrapping causes membrane bending, which increases the elastic energy. The membrane molecules are highly mobile. When the local elastic energy density is large enough to overcome γ_{mw}, the membrane molecules may diffuse to cause hole formation, as shown in Fig. 1(b). The subsequent evolution will be affected by the exposed dendrimer/water interface in the hole. Thus, the competition between interfacial and elastic energies and the elastic energy relaxation lead to the morphological change and hole formation.

We propose a three-dimensional phase-field model to account for the dynamic interaction of the energetics discussed above and the resulting morphological changes. The dendrimer particle, membrane, and water are treated as three phases. Denote the volume fractions of the dendrimer and membrane phases in water by two spatially continuous and time-dependent functions $c_1=c_1(\mathbf{x},t)$ and $c_2=c_2(\mathbf{x},t)$, where t is time and $\mathbf{x}$ is a position vector. The water phase is described by $1-c_1-c_2$. Note that $c_1(\mathbf{x},t)\sim 1$, $c_2(\mathbf{x},t)\sim 0$ in the dendrimer phase, and $c_1(\mathbf{x},t)\sim 0$, $c_2(\mathbf{x},t)\sim 1$ in the membrane phase.

The total free energy depends on the phase configuration. Here, we integrate the chemical energy, interfacial energy, and the bending energy. The total free energy is given by

$$G = G_c + G_i + G_b, \tag{1}$$

where G_c is the bulk chemical energy, G_i the interfacial energy, and G_b the elastic bending energy. The chemical energy is given by

$$G_c = \int_V f(c_1,c_2)dV, \tag{2}$$

where V extends over the system volume. This energy drives phase separation. For the ternary system, we adopt the Mug-

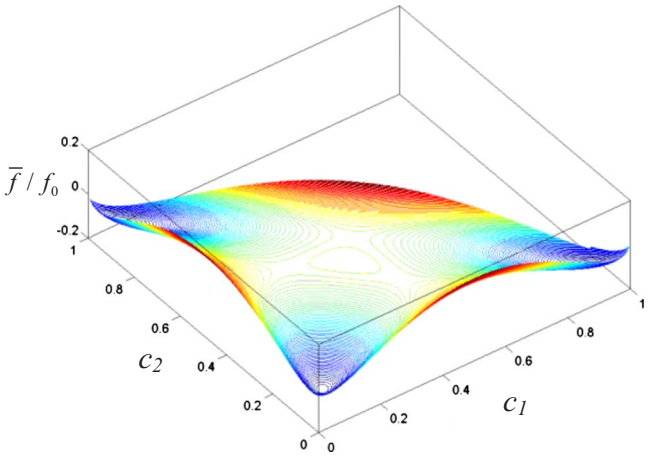

FIG. 2. (Color online) The chemical energy function shows three wells corresponding to three phases.

gianu's form [16] $f(c_1,c_2)=c_1f_d+c_2f_m+(1-c_1-c_2)f_w+\bar{f}$, where

$$\begin{aligned}\bar{f}(c_1,c_2) = f_0\{&c_1 \ln c_1 + c_2 \ln c_2 + (1-c_1-c_2)\ln(1-c_1-c_2)\\ &+ c_1c_2[\Omega_{12}^0 + \Omega_{12}^1(c_1-c_2)] + c_2(1-c_1-c_2)[\Omega_{23}^0\\ &+ \Omega_{23}^1(c_1+2c_2-1)] + c_1(1-c_1-c_2)[\Omega_{13}^0\\ &+ \Omega_{13}^1(2c_1+c_2-1)]\}.\end{aligned} \tag{3}$$

Here f_d, f_m, and f_w denote the chemical energy when the system is composed of a single dendrimer, membrane, or water phase, respectively. The average concentration is constant due to mass conservation, hence the linear term of the free energy does not affect diffusion and can be neglected. In Eq. (3), k_B is Boltzmann's constant, T is the absolute temperature, and Ω_{ij}^0 and Ω_{ij}^1 are parameters that determine the shape of the energy profile. Figure 2 shows an example of $\bar{f}(c_1,c_2)$ with $\Omega_{12}^0=\Omega_{23}^0=\Omega_{13}^0=3.5$ and $\Omega_{12}^1=\Omega_{23}^1=\Omega_{13}^1=1.0$, which has three wells corresponding to the three phases.

The interfacial energy between the dendrimer and membrane, dendrimer and water can be established through the gradient terms of c_1 and c_2,

$$G_i = \int_V (h_{11}(\nabla c_1)^2 + h_{12}\nabla c_1 \cdot \nabla c_2 + h_{22}(\nabla c_2)^2)dV. \tag{4}$$

Here, h_{11}, h_{12}, and h_{22} are material constants. The term $h_{11}(\nabla c_1)^2$ describes the interfacial energy between the dendrimer and water, where the nonuniformity of c_1 increases the energy. Similarly, the term $h_{22}(\nabla c_2)^2$ accounts for the interfacial energy between the membrane and water. Note that the term $h_{12}\nabla c_1\cdot\nabla c_2$ vanishes unless both c_1 and c_2 change in the same region. Thus, it describes the interfacial energy between the dendrimer and membrane. Without loss of generality, consider the concentration change across the interface from the dendrimer side to the membrane side. The concentration c_1 decreases while c_2 increases. Thus $\nabla c_1\cdot\nabla c_2$ is negative in the interfacial region. To describe the interfacial energy, the parameter h_{12} should be a negative constant so that $h_{12}\nabla c_1\cdot\nabla c_2>0$. However, here we have lumped the

charge interaction between the dendrimer and membrane into the interfacial energy term. When the charge attraction is larger than the physical interfacial energy, the formation of a dendrimer/membrane interface actually reduces the energy. This leads to an effective negative interface tension or a positive h_{12}.

The elastic bending energy of a membrane is given by $G_b = 1/2\int_A K_B(2H)^2 dA$.[17] Here, K_B is the bending stiffness and H is the mean curvature. The integration extends over the middle plane of the membrane. As shown in the Appendix, we can express the elastic energy in the membrane as

$$G_b = \frac{3}{2\sqrt{2}}\tau K_B \int_V \left\{ \nabla^2 c_2 + \frac{(c_2 - 1/2)}{\tau^2}[1 - 4(c_2 - 1/2)^2] \right\}^2 dV, \tag{5}$$

where τ is a tunable artificial interface thickness. The determination of τ in computations depends on the resolution to be resolved and consideration of the computational cost.

The chemical potential of each phase is given by $\mu_1 = \delta G/\delta c_1$ and $\mu_2 = \delta G/\delta c_2$, respectively. The application of Eqs. (1)–(5) leads to

$$\mu_1 = f_0 p_1 - 2h_{11}\nabla^2 c_1 - h_{12}\nabla^2 c_2, \tag{6}$$

$$\mu_2 = f_0 p_2 - 2h_{22}\nabla^2 c_2 - h_{12}\nabla^2 c_1 + K_B g_1 + K_B \nabla^2 g_2, \tag{7}$$

where

$$p_1 = \ln\left(\frac{c_1}{1 - c_1 - c_2}\right) + \Omega_{12}^0 c_2 + \Omega_{12}^1 (2c_1 c_2 - c_2^2) - \Omega_{23}^0 c_2 + \Omega_{23}^1 (-2c_1 c_2 - 3c_2^2 + 2c_2) + \Omega_{13}^0 (1 - 2c_1 - c_2) - \Omega_{13}^1 (1 - 6c_1 + 6c_1^2 - 2c_2 + 6c_1 c_2 + c_2^2), \tag{8}$$

$$p_2 = \ln\left(\frac{c_2}{1 - c_1 - c_2}\right) + \Omega_{12}^0 c_1 + \Omega_{12}^1 (c_1^2 - 2c_1 c_2) + \Omega_{23}^0 (1 - c_1 - 2c_2) + \Omega_{23}^1 (-1 + 2c_1 - c_1^2 + 6c_2 - 6c_1 c_2 - 6c_2^2) - \Omega_{13}^0 c_1 - \Omega_{13}^1 (3c_1^2 + 2c_1 c_2 - 2c_1), \tag{9}$$

$$g_1 = \frac{3\sqrt{2}}{\tau^3}(1 - 6c_2 + 6c_2^2)(2c_2 - 6c_2^2 + 4c_2^3 - \tau^2 \nabla^2 c_2), \tag{10}$$

$$g_2 = \frac{3\sqrt{2}}{2\tau}(-2c_2 + 6c_2^2 - 4c_2^3 + \tau^2 \nabla^2 c_2). \tag{11}$$

The mass conservation requires that the time rate of the concentration compensates the divergence of the flux vector, $\mathbf{J}_1$, $\mathbf{J}_2$, namely $\partial c_1/\partial t = -\nabla \cdot \mathbf{J}_1$ and $\partial c_2/\partial t = -\nabla \cdot \mathbf{J}_2$. Following Cahn and Hilliard [18], we assume that the flux is linearly proportional to the driving forces $\mathbf{F}_1 = -\nabla \mu_1$ and $\mathbf{F}_2 = -\nabla \mu_2$. Diffusion flux from the mass transport is given by $\mathbf{J}_1 = M\mathbf{F}_1$ and $\mathbf{J}_2 = M\mathbf{F}_2$, where M is the mobility. This relationship together with the mass conservation yields the following diffusion equations:

$$\frac{\partial c_1}{\partial t} = \nabla(M \nabla \mu_1), \tag{12}$$

$$\frac{\partial c_2}{\partial t} = \nabla(M \nabla \mu_2). \tag{13}$$

III. NUMERICAL PROCEDURES

To resolve the interface, we choose the characteristic length to be τ. The time scale is defined by $t_c = \tau^2/(Mf_0)$. We normalize Eqs. (6), (7), (12), and (13) by the characteristic length and time. The normalized equations become

$$\frac{\partial c_1}{\partial t} = \nabla^2 \mu_1, \tag{14}$$

$$\frac{\partial c_2}{\partial t} = \nabla^2 \mu_2, \tag{15}$$

$$\mu_1 = p_1 - 2C_{11}^2 \nabla^2 c_1 - C_{12}^2 \nabla^2 c_2, \tag{16}$$

$$\mu_2 = p_2 - 2C_{22}^2 \nabla^2 c_2 - C_{12}^2 \nabla^2 c_1 + \kappa_B q_1 + \kappa_B \nabla^2 q_2, \tag{17}$$

where

$$C_{11} = \sqrt{h_{11}/f_0}/\tau, \quad C_{12} = \sqrt{h_{12}/f_0}/\tau, \quad C_{22} = \sqrt{h_{22}/f_0}/\tau,$$

$$q_1 = 3\sqrt{2}(1 - 6c_2 + 6c_2^2)(2c_2 - 6c_2^2 + 4c_2^3 - \nabla^2 c_2),$$

$$q_2 = 3\sqrt{2}(-2c_2 + 6c_2^2 - 4c_2^3 + \nabla^2 c_2)/2,$$

$$\kappa_B = K_B/(f_0 \tau^3).$$

Applying the explicit forward Euler method for the time integration in Eqs. (14) and (15) requires very small time step to maintain the numerical stability. Instead, we adopted a semi-implicit scheme [19]. The key idea is to treat the linear term implicitly and the nonlinear term explicitly to allow for larger time steps without losing numerical stability. Take Eq. (14) as an example. To evolve the equation from time n to $n+1$ at time step Δt, we can express $\partial c_1/\partial t = (c_1^{n+1} - c_1^n)/\Delta t$ and $\nabla^2 \mu_1 = \nabla^2 p_1^n - 2C_{11}^2 \nabla^4 c_1^{n+1} - C_{12}^2 \nabla^4 c_2^{n+1}$. Equation (15) can be discretized in the same way. The discrete form is given by

$$\left(\frac{1}{\Delta t} + 2C_{11}^2 \nabla^4\right) c_1^{n+1} + C_{12}^2 \nabla^4 c_2^{n+1} = \frac{1}{\Delta t} c_1^n + \nabla^2 p_1^n, \tag{18}$$

$$C_{12}^2 \nabla^4 c_1^{n+1} + \left(\frac{1}{\Delta t} + 2C_{22}^2 \nabla^4\right) c_2^{n+1} = \frac{1}{\Delta t} c_2^n + \nabla^2 p_2^n + \kappa_B \nabla^2 q_1^n + \kappa_B \nabla^4 q_2^n. \tag{19}$$

The equations can be solved with high spatial resolution efficiently in Fourier space. Applying Fourier transform to both sides of Eqs. (18) and (19), we obtain

$$\begin{pmatrix} \hat{c}_1^{n+1} \\ \hat{c}_2^{n+1} \end{pmatrix} = \begin{bmatrix} 1/\Delta t + 2C_{11}^2 k^4 & C_{12}^2 k^4 \\ C_{12}^2 k^4 & 1/\Delta t + 2C_{22}^2 k^4 \end{bmatrix}^{-1} \begin{pmatrix} \hat{c}_1^n/\Delta t - k^2 \hat{p}_1^n \\ \hat{c}_2^n/\Delta t - k^2 \hat{p}_2^n - \kappa_B k^2 \hat{q}_1^n + \kappa_B k^4 \hat{q}_2^n \end{pmatrix}, \tag{20}$$

where the caret ^ stands for Fourier transform. The vector $\mathbf{k}$ denotes the wave vector in Fourier space with $k^2 = k_1^2 + k_2^2 + k_3^2$.

IV. RESULTS AND DISCUSSIONS

All the simulations were performed on a $64 \times 64 \times 32$ domain measured in length τ. To resolve the interface, we took $\tau = 1$ nm to normalize the length. The initial configuration was a dendrimer particle just in contact with a lipid layer. We used a diameter of 8 for G7 dendrimers and 5 for G5 dendrimers. We took five for the thickness of the lipid layer, which is consistent with the dimyristorylphospatidylchonline (DMPC) membrane. For the chemical energy, we set $\Omega_{12}^0 = \Omega_{23}^0 = \Omega_{13}^0 = 3.5$ and $\Omega_{12}^1 = \Omega_{23}^1 = \Omega_{13}^1 = 1.0$. These parameters represent a function with three wells as shown in Fig. 2.

In the phase-field model, the interface thickness is given by $\tau = \sqrt{h_{22}/W}$, where W is the barrier height between the two wells in the free-energy function. [18] In our model, $W \sim 0.2 f_0$. Consider the interface between the membrane and water. As shown in the Appendix, the interface profile is given by a form of $c_2(z) = \{\tanh[z/(\sqrt{2}\tau)] + 1\}/2$. The interfacial tension can be calculated by an integration across the interface, namely,

$$\gamma_{mw} = \int_{-\infty}^{\infty} h_{22} \left(\frac{\partial c_2}{\partial z} \right)^2 dz = \frac{\sqrt{2} h_{22}}{6\tau} \sim 0.1 \sqrt{h_{22} f_0}. \tag{21}$$

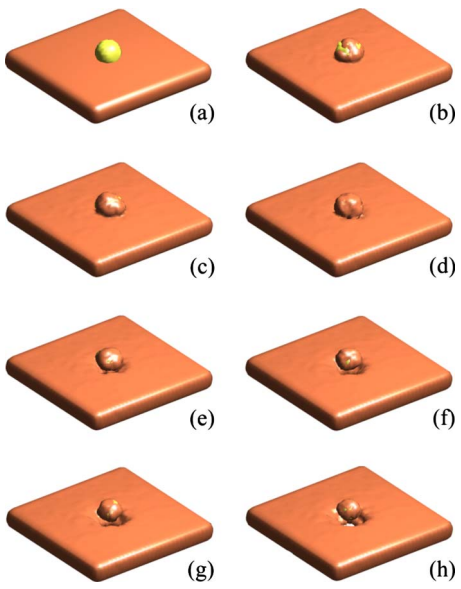

FIG. 3. (Color online) Evolution of the membrane in contact with a G7 amine-terminated dendrimer. (a) $t=0$, (b) $t=2$, (c) $t=4$, (d) $t=6$, (e) $t=8$, (f) $t=10$, (g) $t=12$, and (h) $t=14$.

The interfacial tension for the dendrimer [20] and membrane [21] is approximately $\gamma_{dw} \sim 7.3 \times 10^{-2}$ J/m^2 and $\gamma_{mw} \sim 4.2 \times 10^{-2}$ J/m^2 (DMPC lipid layer), respectively. With $\tau \sim \sqrt{h_{22}/0.2 f_0} = 1$ nm and Eq. (21), we get $f_0 \sim 9.4 \times 10^8$ J/m^3, $h_{22} \sim 1.9 \times 10^{-10}$ J/m, and similarly $h_{11} \sim 5.7 \times 10^{-10}$ J/m. These values give $C_{11} = 0.78$ and $C_{22} = 0.45$. The bending stiffness for a DMPC lipid layer is about $K_B = 5.6 \times 10^{-20}$ J [22] or $\kappa_B \sim 0.06$.

Depending on the surface termination, dendrimers can carry charges. The PAMAM dendrimers with amine-terminated (R-NH$_2$) branches carry positive charges. The surface primary amines have been determined to be protonated at pH$<$7 [23,24]. Acetamide-terminated [R-NHC(0)CH$_3$] dendrimers have neutral surface charges. The DMPC lipid in this simulation is zwitterionic, which means that it carries both positive and negative charges. The configuration yields a net neutral charge on its head. The negative charge of the head-group dipole is linked to the lipid chains that are firmly anchored in the hydrocarbon core of the lipid layer. Hence, this charge can be considered immobile as compared to the positively charged end of the head-group dipole which can move according to the conformational freedom of the head group [25]. Consequently, the dendrimer and membrane attract each other due to the attraction between the positive charge at the surface of the dendrimer and the negative charge at the membrane. The elastic stiffness of the membrane is much smaller compared to that of the dendrimer. Thus, the membrane tends to wrap the dendrimer to reduce the electrostatic energy. In this study, we vary the parameter C_{12} to mimic the role of surface charges instead of solving the electric field directly. We vary it from 0.9 (amine terminated) to 1.7 (acetamide terminated). This variation is expected to mimic experiments involving amine-terminated dendrimers carrying positive charges.

Representative results for G7-amine PAMMA dendrimers are shown in Fig. 3. Experiments showed that adding G7-amine PAMAM dendrimers to the lipid layer caused the formation of small, isolated holes. Our simulations have demonstrated similar hole-formation behavior. As the dendrimer and the lipid layer contact, the strong attraction between the surface of the dendrimer and the lipid layer causes the lipid layer to move toward and subsequently enclose the dendrimer. During this process, the elastic energy increases due to the bending of the membrane. When the energy density is large enough, the bonding between the membrane molecules is broken so that they are pulled away from the original membrane. This process eventually leads to hole formation as shown in Fig. 3(h). The shown behavior is consistent with the postulate proposed by Mecke *et al.* [9]. They argued that dendrimers pull lipid molecules off the substrate, leading to the formation of dendrimer-filled vesicles. However, the vesicles were no longer attached to the substrate and thus could not be experimentally imaged by an AFM tip. Our

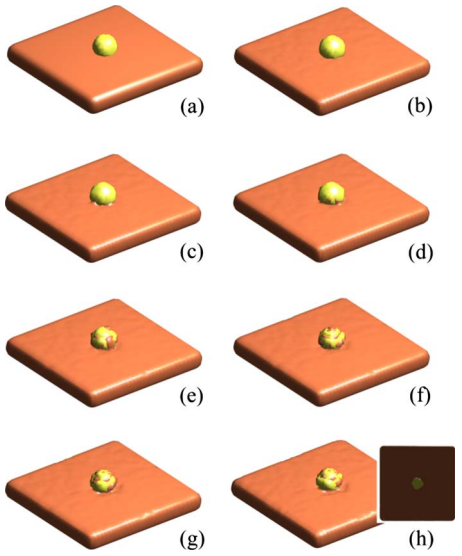

FIG. 4. (Color online) Evolution of the membrane in contact with a G7 acetamide-terminated dendrimer. The inset in (h) shows the hole viewed from the bottom. (a) $t=0$, (b) $t=2$, (c) $t=4$, (d) $t=6$, (e) $t=8$, (f) $t=10$, (g) $t=12$, and (h) $t=14$.

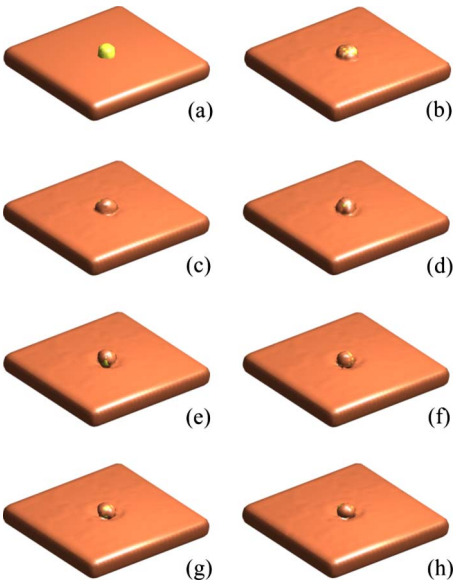

FIG. 5. (Color online) Evolution of the membrane in contact with a G5 amine-terminated dendrimer. (a) $t=0$, (b) $t=2$, (c) $t=4$, (d) $t=6$, (e) $t=8$, (f) $t=10$, (g) $t=12$, and (h) $t=14$.

simulations showed that energetic interactions can drive dendrimer-filled vesicles to self-assemble.

Experiments showed that G7-acetamide PAMAM dendrimers, which are neutrally charged, similarly caused hole formation but resulted in a lower density of holes than G7 amine. This trend has also been observed in our simulations. A comparison of Figs. 3 and 4 shows that the hole generated by G7 acetamide is smaller than that by G7 amine. Although there is no strong charge interaction between the neutral G7 acetamide and the membrane, the adhesive force from van der Waals interaction may still overcome the elastic energy and cohesion of molecules when the dendrimer is large enough. Then, the dendrimer pulls the molecules off the membrane, but the amount of pulled-off molecules is smaller compared to the case of G7 amine.

Experiments suggested that the size of the dendrimer is an important factor in the interaction between dendrimers and lipid layers. A lower-generation G5-amine dendrimer had significantly reduced ability to remove lipid molecules from the membrane. Although G5-amine dendrimer could still remove the lipid layer, it did so more slowly and mostly from the edges of existing defects. Our simulations have demonstrated similar tendencies. As can be seen in Fig. 5, the hole formation by G5 dendrimer starts later than that by G7 dendrimer. The size is also much smaller. In order to form enough stabilizing bonds between the end group of the dendrimer and the lipid molecules, the average number of lipid head groups per dendrimer end group should be small [9]. In other words, the number of lipid head group for one dendrimer end group to pull off should be small. For a G7 PAMAM dendrimer, this value is between 1 and 3. However, the value reaches 6 for a G5 PAMAM dendrimer [9], which implies that a lower generation cannot remove the lipid molecules from the membrane.

Figure 6 shows the effect of a pre-existing defect. The size of the hole generated from the edges of the defect is larger than that from the intact part. G5-acetamide PAMAM dendrimers barely cause the formation or expansion of defects in the lipid layer. Instead, they cause the formation of ledges. In the simulations shown in Fig. 7, the size of hole is very small and there is a well near the dendrimer.

The interaction between a single dendrimer and the lipid layer is not strong enough to create a large hole in the layer. We envision that a group of dendrimers, when they are relatively close, may generate strong collective effects to induce large holes. The simulations in Fig. 8 confirmed the hypothesis. Considering the repulsive forces between dendrimers due to their surface charges, we placed them separately next to each other. The hole induced by the group is much larger than that induced by a single dendrimer.

V. CONCLUSIONS

In this paper, we have proposed and implemented a phase field model to account for the interaction between dendrim-

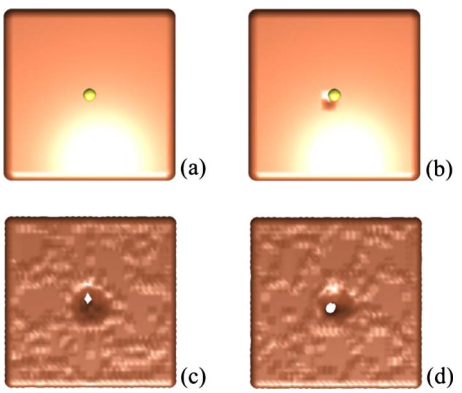

FIG. 6. (Color online) The effect of an existing defect. (a) and (b) are initial configurations. After $t=6$, the hole formed at the pre-existing defect (d) is larger than the hole formed at the intact part (c).

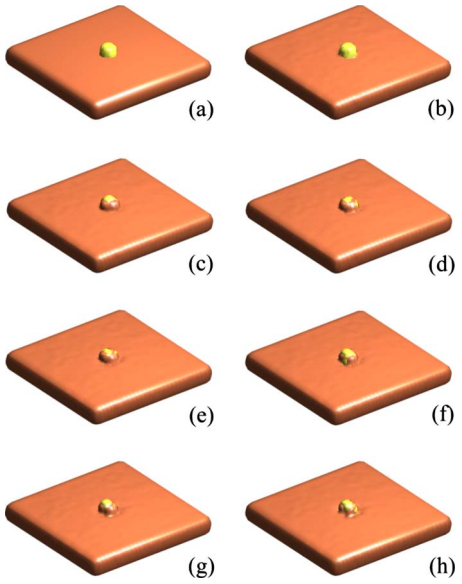

FIG. 7. (Color online) Evolution of the membrane in contact with a G5 acetamide-terminated dendrimer. (a) $t=0$, (b) $t=2$, (c) $t=4$, (d) $t=6$, (e) $t=8$, (f) $t=10$, (g) $t=12$, and (h) $t=14$.

ers and lipid layers and the induced morphology evolutions. Our simulations show that the G7 amine PAMAM dendrimer, which is positively charged, causes hole formation in the membrane. The G7-acetamide PAMAM dendrimer, which is neutrally charged, also causes hole formation but results in a smaller size. These behaviors are consistent with experimental observations. Our simulations suggest that the size of the dendrimer is another important factor. Lower-generation dendrimers which have smaller sizes exhibit significantly reduced ability to remove lipid molecules from the membrane. It is shown that pre-existing defects on the lipid layer can be expanded by a dendrimer. Multiple dendrimers can lead to large holes not achievable by a single dendrimer.

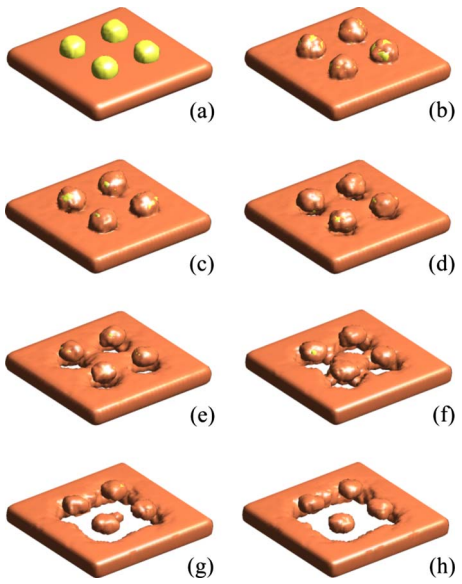

FIG. 8. (Color online) Multiple dendrimers induce a large hole. Shown for $t=4$.

Highlighting the competing actions of multiple concurrent energetic forces, the model may help provide critical insight into the nanoparticle design for various biological and medicinal applications.

ACKNOWLEDGMENT

The authors acknowledge financial support from the National Science Foundation under No. DMI-0348375.

APPENDIX

Consider a domain V described by a phase-field variable $c(\mathbf{x})$. Two phases are represented by $c=1$ and $c=0$, respectively. Denote the phase boundary by A. The field variable can be expressed in terms of a signed-distance function, $d(\mathbf{x})$. The signed-distance function determines how close a given point $\mathbf{x}$ is to the boundary. The function satisfies $d(\mathbf{x})=0$ for $\mathbf{x}\in A$, is the negative distance for $\mathbf{x}$ inside one phase, and is the positive distance for $\mathbf{x}$ inside the other phase. The phase field $c(\mathbf{x})$ can be expressed by [15]

$$c(\mathbf{x}) = \frac{1}{2}\left(\tanh\left[\frac{d(\mathbf{x})}{\sqrt{2}\tau}\right]+1\right) = g\left(\frac{d(\mathbf{x})}{\sqrt{2}\tau}\right), \tag{A1}$$

where τ denotes the interface thickness. From the relations $\tanh'(\,)=1-\tanh^2(\,)$, $\tanh''(\,)=-2\tanh(\,)[1-\tanh^2(\,)]$, we have

$$g' = \frac{1}{2}\left[1-4\left(g-\frac{1}{2}\right)^2\right],\quad g'' = -2\left(g-\frac{1}{2}\right)\left[1-4\left(g-\frac{1}{2}\right)^2\right]. \tag{A2}$$

From Eq. (A1), we have

$$\nabla c = g'\frac{\nabla d}{\sqrt{2}\tau},\quad \nabla^2 c = g''\frac{(\nabla d)^2}{2\tau^2}+g'\frac{\nabla^2 d}{\sqrt{2}\tau}. \tag{A3}$$

The normal vector of the interface is given by $\mathbf{n}=\nabla d=\sqrt{2}\tau\nabla c/g'$, which satisfies $\mathbf{n}\cdot\mathbf{n}=(\nabla d)^2=1$. From Eq. (A3), we have

$$\nabla^2 d = \frac{\sqrt{2}\tau}{g'}\left(\nabla^2 c-\frac{g''}{2\tau^2}\right). \tag{A4}$$

The mean curvature H can be written in terms of the phase-field variable $c(\mathbf{x})$ as

$$H = \frac{1}{2}\nabla\cdot\mathbf{n} = \frac{1}{2}\nabla^2 d = \frac{\sqrt{2}\tau}{2g'}\left(\nabla^2 c-\frac{g''}{2\tau^2}\right)$$
$$= \frac{\sqrt{2}\tau}{1-4\left(c-\frac{1}{2}\right)^2}\left\{\nabla^2 c+\frac{\left(c-\frac{1}{2}\right)}{\tau^2}\left[1-4\left(c-\frac{1}{2}\right)^2\right]\right\}. \tag{A5}$$

A membrane has two interfaces A_1 and A_2. Denote the middle plane by A. The bending energy is given by

$$G_b = \frac{1}{2}\int_A K_B(2H)^2 dA, \tag{A6}$$

where H is the curvature of the middle plane. Here, we average the calculation by using the curvatures at the two interfaces, H_1 and H_2, namely,

$$G_b = \frac{G_{b1}+G_{b2}}{2} = \frac{1}{4}\int_{A_1} K_B(2H_1)^2 dA + \frac{1}{4}\int_{A_2} K_B(2H_2)^2 dA. \tag{A7}$$

Now consider only one interface A_1 in the domain. Using the relation $\int_{-\infty}^{+\infty}[1-\tanh^2(z/\sqrt{2}\tau)]^2 dz = 4\sqrt{2}\tau/3$ and multiple it to G_{b1}, we can rewrite

$$G_{b1} = \frac{3}{4\sqrt{2}\tau}\int_{-\infty}^{+\infty}\left[1-\tanh^2\left(\frac{z}{\sqrt{2}\tau}\right)\right]^2 dz \int_{A_1}\frac{K_B}{2}(2H_1)^2 dA. \tag{A8}$$

Choose z to be normal to A_1. The form in Eq. (A8) can be expressed by a volume integration

$$G_{b1} = \frac{3}{\sqrt{2}}\tau K_B \int_V \left\{\nabla^2 c + \frac{(c-1/2)}{\tau^2}[1-4(c-1/2)^2]\right\}^2 dV. \tag{A9}$$

Similar expression exists for G_{b2}. For a membrane, both A_1 and A_2 exist; the integration of z from $-\infty$ to ∞ includes both interfaces. Thus we have

$$G_b = \frac{3}{2\sqrt{2}}\tau K_B \int_V \left\{\nabla^2 c + \frac{(c-1/2)}{\tau^2}[1-4(c-1/2)^2]\right\}^2 dV. \tag{A10}$$

[1] J. R. Baker, A. Quintana, L. Piehler, M. M. Holl, D. A. Tomalia, and E. Raczka, Biomed. Microdevices **3**, 61 (2001).
[2] N. Malik, E. G. Evagorou, and R. Duncan, Anti-Cancer Drugs **10**, 767 (1999).
[3] I. J. Majoros, T. P. Thomas, C. B. Mehta, and J. R. Baker, J. Med. Chem. **48**, 5892 (2005).
[4] S. Hong, P. R. Leroueli, I. Majoros, B. G. Orr, and J. R. Baker, Chem. Biol. **14**, 107 (2007).
[5] N. Karoonuthaisiri, K. Titiyevskiy, and J. L. Thomas, Colloids Surf., B **27**, 365 (2003).
[6] M. F. Ottaviani, P. Favuzza, B. Sacchi, N. J. Turro, S. Jockusch, and D. A. Tomalia, Langmuir **18**, 2347 (2002).
[7] S. Hong, A. U. Bielinska, M. A. B. Keszler, J. L. Beals, X. Shi, L. Balogh, B. G. Orr, J. R. Baker, and M. M. B. Holl, Bioconjugate Chem. **15**, 774 (2004).
[8] S. Hong, P. R. Leroueil, E. K. Janus, J. L. Peters, M. Kober, M. T. Islam, B. G. Orr, J. R. Baker, and M. M. B. Holl, Bioconjugate Chem. **17**, 728 (2006).
[9] A. Mecke, I. J. Majoros, A. K. Patri, J. R. Baker, M. M. B. Holl, and B. G. Orr, Langmuir **21**, 10348 (2005).
[10] P. J. Bond and M. S. P. Sansom, J. Am. Chem. Soc. **128**, 2697 (2006).
[11] P. K. Maiti, T. Cagin, S. T. Lin, and W. A. Goddard, Macromolecules **38**, 979 (2005).
[12] H. Lee and R. G. Larson, J. Phys. Chem. B **110**, 18204 (2006).
[13] W. Lu and Z. Suo, J. Mech. Phys. Solids **49**, 1937 (2001).
[14] D. Kim and W. Lu, Phys. Rev. B **73**, 035206 (2006).
[15] Q. Du, C. Liu, and X. Wang, J. Comput. Phys. **198**, 450 (2004).
[16] N. Saunders and A. P. Miodounik, *CALPHAD (Calculation of Phase Diagram): A Comprehensive Guide* (Pergamon Press, New York, 1998).
[17] W. Helfrich, Z. Naturforsch. [C] **28**, 693 (1973).
[18] J. W. Cahn and J. E. Hilliard, J. Chem. Phys. **28**, 258 (1958).
[19] L.-Q. Chen and J. Shen, Comput. Phys. Commun. **108**, 147 (1998).
[20] R. C. Triulzi, M. Micic, J. Orbulescu, S. Giordani, B. Mueller, and R. M. Leblanc, Analyst (Cambridge, U.K.) **133**, 667 (2008).
[21] J. Henin and C. Chipot, Chem. Phys. Lett. **425**, 329 (2006).
[22] E. Evans and W. Rawicz, Phys. Rev. Lett. **64**, 2094 (1990).
[23] M. F. Ottaviani, F. Montalti, M. Romanelli, N. J. Turro, and D. A. Tomalia, J. Phys. Chem. **100**, 11033 (1996).
[24] R. C. v. Duijvenbode, M. Borkovec, and G. J. M. Koper, Polymer **39**, 2657 (1998).
[25] E. C. Mbamala, A. B. Shaul, and S. May, Biophys. J. **88**, 1702 (2005).